

32 **from Lu et al. (2007) show that the gravimetric fraction of sand is a better predictor of f_q**
33 **when a larger variety of soil types is considered.**

34
35
36
37
38
39 **1. Introduction**

40

41 Soil moisture is the main driver of temporal changes in values of the soil thermal conductivity.
42 The latter is a key variable in land surface models (LSMs) used in hydrometeorology, for the
43 simulation of the vertical profile of soil temperature in relation to soil moisture. Shortcomings in
44 soil thermal conductivity models tend to limit the impact of improving the simulation of soil
45 moisture in LSMs. Models of the thermal conductivity of soils are affected by uncertainties,
46 especially in the representation of the impact of soil properties such as the volumetric fraction of
47 quartz (f_q), soil organic matter, and gravels. As soil organic matter and gravels are often neglected
48 in LSMs, the soil thermal conductivity models used in most LSMs represent the mineral fine
49 earth, only. Today, f_q estimates are not given in global digital soil maps and it is often assumed
50 that this quantity is equal to the fraction of sand.

51 Soil thermal properties are characterized by two key variables: the soil volumetric heat capacity
52 (C_h), and the soil thermal conductivity (λ), in $\text{Jm}^{-3}\text{K}^{-1}$ and $\text{Wm}^{-1}\text{K}^{-1}$, respectively. Provided the
53 volumetric fractions of moisture, minerals and organic matter are known, C_h can be calculated
54 easily. On the other hand, the estimation of λ relies on empirical models and is affected by
55 uncertainties (Peters-Lidard et al., 1998 ; Tarnawski et al., 2012). The construction and the
56 verification of the λ models is not easy as λ is often measured in the lab on perturbed soil
57 samples (Abu-Hamdeh et al., 2000; Lu et al., 2007). Although recent advances in line-source

58 probe and heat pulse methods have made it easier to monitor soil thermal conductivity in the field
59 (Bristow et al., 1994; Zhang et al., 2014), such measurements are currently not made in
60 operational meteorological networks. Moreover, for given soil moisture conditions, λ depends to
61 a large extent on the fraction of soil minerals presenting high thermal conductivities such as
62 quartz, hematite, dolomite or pyrite (Côté and Conrad, 2005). At mid-latitudes, quartz is the main
63 driver of λ . The information on quartz fraction in a soil is usually unavailable as it can only be
64 measured using X-ray diffraction or X-ray fluorescence techniques, which are difficult to
65 implement (Schönenberger et al., 2012). This has a major effect on the accuracy of thermal
66 conductivity models and their applications (Bristow, 1998).

67 Today, most of the Land Surface Models (LSMs) used in meteorology and hydrometeorology
68 simulate λ following the approach proposed by Peters-Lidard et al. (1998). This approach
69 consists of an updated version of the Johansen (1975) model, and assumes that the gravimetric
70 fraction of quartz (Q) is equal to the gravimetric fraction of sand within mineral fine earth. This is
71 a strong assumption, as some sandy soils (e.g. calcareous sands) may contain little quartz, and as
72 quartz may be found in the silt and clay fractions of the soil minerals. Moreover, soil organic
73 matter (SOM) and gravels are often neglected in LSMs, and the λ models used in most LSMs
74 represent the mineral fine earth, only. Yang et al. (2005) and Chen et al. (2012) have shown the
75 importance of accounting for SOM and gravels in λ models for organic top soil layers of
76 grasslands of the Tibetan plateau.

77 In this study, an attempt is made to use routine automatic soil temperature sub-hourly
78 measurements to retrieve instantaneous soil thermal diffusivity values at 21 weather stations of
79 the Soil Moisture Observing System – Meteorological Automatic Network Integrated Application
80 (SMOSMANIA) network (Calvet et al., 2007) in southern France, at a depth of 0.10 m. Using

81 information on soil moisture, soil texture, soil gravel content, soil organic matter, and bulk
82 density, λ values are derived from soil thermal diffusivity and heat capacity. The response of λ to
83 soil moisture is investigated and the feasibility of modelling the λ value at saturation (λ_{sat}) with or
84 without using SOM and gravel fraction observations is assessed using an empirical thermal
85 conductivity model based on Lu et al. (2007). The volumetric fraction of quartz, f_q , is retrieved by
86 reverse modelling together with Q . Pedotransfer functions are further proposed for estimating
87 quartz content from soil texture information.

88 The field data and the method to retrieve λ values are presented in Sect. 2. The λ and f_q retrievals
89 are presented in Sect. 3 together with a sensitivity analysis of λ_{sat} to SOM and gravel fractions.

90 Finally, the results are discussed in Sect. 4, and the main conclusions are summarized in Sect. 5.

91 Technical details are given in Supplements.

92

93

94 **2. Data and methods**

95

96

97 2.1. The SMOSMANIA data

98

99

100 The SMOSMANIA soil moisture network was developed by Calvet et al. (2007) in southern
101 France in order to validate satellite-derived soil moisture products (Parrens et al., 2012), assess
102 land surface models used in hydrological models (Draper et al., 2011) and in meteorological
103 models (Albergel et al., 2010), and monitor the impact of climate change on water resources and
104 droughts. The station network forms a transect between the Atlantic coast and the Mediterranean
105 sea (Fig. 1). It consists of pre-existing automatic weather stations operated by Meteo-France,

106 upgraded with four soil moisture probes at four depths: 0.05 m, 0.10 m, 0.20 m, and 0.30 m. In
107 general, the stations are located on former cultivated fields and consist of grasslands. Soil
108 properties were measured at each stations using soil samples collected during the installation of
109 the probes. The 21 stations cover a very large range of soil texture characteristics (see
110 Supplement 1). Other properties such as the gravimetric fraction of the Soil Organic Matter
111 (SOM) and of gravels were determined from the soil samples. In addition, the bulk dry density of
112 the soil (ρ_d) was measured using unperturbed oven-dried soil samples collected using metal
113 cylinders of known volume (about $7 \times 10^{-4} \text{ m}^3$).

114 Twelve SMOSMANIA stations were activated in 2006 in southwestern France. In 2008, nine
115 more stations were installed along the Mediterranean coast, and the whole network (21 stations)
116 was gradually equipped with temperature sensors at the same depths as soil moisture probes. The
117 soil moisture and soil temperature probes consisted of ThetaProbe ML2X and PT100 sensors,
118 respectively.

119 The ThetaProbe sensors provide a voltage signal in units of V. In order to convert the voltage
120 signal into volumetric soil moisture content ($\text{m}^3 \text{ m}^{-3}$), site-specific calibration curves were
121 developed using in situ gravimetric soil samples for all stations, and for all depths (Albergel et
122 al., 2008). In this study, the calibration was revised in order to avoid spurious high soil moisture
123 values during intense precipitation events. Logistics curves were used (see Supplement 1) instead
124 of exponential curves in the previous version of the data set.

125 The soil temperature observations are recorded with a resolution of 0.1 °C.

126 The observations from the 48 soil moisture probes and from the 48 temperature probes are
127 automatically recorded every 12 minutes. The data are available to the research community
128 through the International Soil Moisture Network web site (<https://ismn.geo.tuwien.ac.at/>).

129 Figure 2 shows soil temperature time series at the Saint-Félix-de-Lauragais (SFL) station on 23
130 February 2015. The impact of recording temperature with a resolution of 0.1 °C is clearly visible
131 at all depths as this causes a levelling of the curves.

132 In this study, sub-hourly measurements of soil temperature and soil moisture at a depth of 0.10 m
133 are used, together with soil temperature measurements at 0.05 m and 0.20 m, from 1 January
134 2008 to 30 September 2015.

135

136 2.2. Soil characteristics

137

138 The porosity values at a depth of 0.10 m are listed in Table 1 together with gravimetric and
139 volumetric fractions of soil particle-size ranges (sand, clay, silt, gravel) and SOM. The porosity,
140 or soil volumetric moisture at saturation (θ_{sat}), is derived from the bulk dry density ρ_d , together
141 with soil texture and soil organic matter observations as:

$$142 \theta_{sat} = 1 - \rho_d \left[\frac{m_{sand} + m_{clay} + m_{silt} + m_{gravel}}{\rho_{min}} + \frac{m_{SOM}}{\rho_{SOM}} \right]$$

143 or

$$144 \theta_{sat} = 1 - f_{sand} - f_{clay} - f_{silt} - f_{gravel} - f_{SOM} \quad (1)$$

145 where m_x (f_x) represents the gravimetric (volumetric) fraction of the soil component x . The f_x
146 values are derived from the measured gravimetric fractions, multiplied by the ratio of ρ_d
147 observations to ρ_x , the density of each soil component x . Values of $\rho_{SOM} = 1300 \text{ kg m}^{-3}$ and $\rho_{min} =$
148 2660 kg m^{-3} are used for soil organic matter, and soil minerals, respectively.

149

150

151 2.3. Retrieval of soil thermal diffusivity

152

153 The soil thermal diffusivity (D_h) is expressed in m^2s^{-1} and is defined as:

154
$$D_h = \frac{\lambda}{C_h} \quad (2)$$

155 In this study, a simple numerical method is used to retrieve instantaneous values of D_h at a depth
156 of 0.10 m using three soil temperature observations at 0.05 m, 0.10 m and 0.20 m, performed
157 every 12 minutes, by solving the Fourier thermal diffusion equation. The latter can be written as:

158
$$C_h \frac{\partial T}{\partial t} = \frac{\partial}{\partial z} \left(\lambda \frac{\partial T}{\partial z} \right) \quad (3).$$

159 In this study, given that soil properties are relatively homogeneous on the vertical (Sect. 2.1),
160 values of D_h can be derived from the Fourier one-dimensional law:

161
$$\frac{\partial T}{\partial t} = D_h \frac{\partial^2 T}{\partial z^2} \quad (4).$$

162 However, large differences in soil bulk density, from the top soil layer to deeper soil layers were
163 observed for some soils (see Supplement 1). In order to limit this effect as much as possible, we
164 only used the soil temperature data presenting a relatively low vertical gradient close to the soil
165 surface, where most differences with deeper layers are found. This data sorting procedure is
166 described in Supplement 2.

167 Given that three soil temperatures T_i (i ranging from 1 to 3) are measured at depths $z_1 = -0.05$ m,
168 $z_2 = -0.10$ m, and $z_3 = -0.20$ m, the soil diffusivity D_{hi} at $z_i = z_2 = -0.10$ m can be obtained by
169 solving the one-dimensional heat equation, using a finite difference method based on the implicit
170 Crank-Nicholson scheme. When three soil depths are considered, z_{i-1} , z_i , z_{i+1} , the change in soil

171 temperature T_i at depth z_i , from time t_{n-1} to time t_n , within the time interval $\Delta t = t_n - t_{n-1}$ can be
 172 written as:

$$173 \frac{T_i^n - T_i^{n-1}}{\Delta t} = D_{hi} \left[\frac{1}{2} \left(\frac{\gamma_{i+1}^n - \gamma_i^n}{\Delta z_m} \right) + \frac{1}{2} \left(\frac{\gamma_{i+1}^{n-1} - \gamma_i^{n-1}}{\Delta z_m} \right) \right] \text{ with}$$

$$174 \gamma_i^n = \frac{T_i^n - T_{i-1}^n}{\Delta z_i}, \Delta z_m = \frac{\Delta z_i + \Delta z_{i+1}}{2}, \text{ and } \Delta z_i = z_i - z_{i-1} \quad (5).$$

175
 176 In this study, $\Delta z_i = -0.05$ m, $\Delta z_{i+1} = -0.10$ m, and a value of $\Delta t = 2880$ s (48 minutes) is used.

177 It is important to ensure that D_h retrievals are related to diffusion processes only and not to the
 178 transport of heat by water infiltration or evaporation (Parlange et al., 1998 ; Schelde et al., 1998).

179 Therefore, only situations for which changes in soil moisture at all depths do not exceed 0.001
 180 m^3m^{-3} within the Δt time lag are considered.

181

182 2.4. From soil diffusivity to soil thermal conductivity

183
 184
 185 The observed soil properties and volumetric soil moisture are used to calculate the soil
 186 volumetric heat capacity C_h at a depth of 0.10 m, using the de Vries (1963) mixing model. The C_h
 187 values, in units of $\text{Jm}^{-3}\text{K}^{-1}$, are calculated as:

$$188 C_h = \theta C_{h\text{water}} + f_{\min} C_{h\min} + f_{SOM} C_{hSOM} \quad (6)$$

189 where θ and f_{\min} represent the volumetric soil moisture and the volumetric fraction of soil
 190 minerals, respectively. Values of $4.2 \times 10^6 \text{ Jm}^{-3}\text{K}^{-1}$, $2.0 \times 10^6 \text{ Jm}^{-3}\text{K}^{-1}$, and $2.5 \times 10^6 \text{ Jm}^{-3}\text{K}^{-1}$, are used
 191 for $C_{h\text{water}}$, $C_{h\min}$, C_{hSOM} , respectively.

192 The λ values at 0.10 m are then derived from the D_h and C_h estimates (Eq. (2)).

193

194 2.5. Soil thermal conductivity model

195

196 In dry conditions, soils present low thermal conductivity values (λ_{dry}). Experimental evidence

197 show that λ_{dry} is negatively correlated with porosity. For example, Lu et al. (2007) give:

$$198 \quad \lambda_{dry} = 0.51 - 0.56 \times \theta_{sat} \quad (\text{in } \text{Wm}^{-1}\text{K}^{-1}) \quad (7)$$

199 When soil pores are gradually filled with water, λ tends to increase towards a maximum value at

200 saturation (λ_{sat}). Between dry and saturation conditions, λ is expressed as:

$$201 \quad \lambda = \lambda_{dry} + K_e (\lambda_{sat} - \lambda_{dry}) \quad (8)$$

202 where, K_e is the Kersten number. The latter is related to the volumetric soil moisture, θ , i.e. to the

203 degree of saturation (S_d). In this study, the formula recommended by Lu et al. (2007) is used:

$$204 \quad K_e = \exp\left\{\alpha\left(1 - S_d^{(\alpha-1.33)}\right)\right\},$$

205 with $\alpha = 0.96$ for $Mn_{sand} \geq 0.4 \text{ kg kg}^{-1}$, $\alpha = 0.27$ for $Mn_{sand} < 0.4 \text{ kg kg}^{-1}$, and

$$206 \quad S_d = \theta / \theta_{sat} \quad (9).$$

207 Mn_{sand} represents the sand mass fraction of mineral fine earth (values are given in Supplement 1).

208 Following Peters-Lidard et al. (1998), λ_{other} is taken as $2.0 \text{ Wm}^{-1}\text{K}^{-1}$ for soils with $Mn_{sand} > 0.2$

209 kg kg^{-1} , and $3.0 \text{ Wm}^{-1}\text{K}^{-1}$ otherwise. In this study $Mn_{sand} > 0.2 \text{ kg kg}^{-1}$ for all soils, except for

210 URG, PRG, and CDM.

211 The geometric mean equation for λ_{sat} proposed by Johansen (1975) for the mineral components

212 of the soil can be generalized to include the SOM thermal conductivity (Chen et al., 2012) as:

213 $\ln(\lambda_{sat}) = f_q \ln(\lambda_q) + f_{other} \ln(\lambda_{other}) + \theta_{sat} \ln(\lambda_{water}) + f_{SOM} \ln(\lambda_{SOM})$
 214
 215 (10)

216 where f_q is the volumetric fraction of quartz, and $\lambda_q = 7.7 \text{ Wm}^{-1}\text{K}^{-1}$, $\lambda_{other} = 2.0 \text{ Wm}^{-1}\text{K}^{-1}$, λ_{water}
 217 $= 0.594 \text{ Wm}^{-1}\text{K}^{-1}$, $\lambda_{SOM} = 0.25 \text{ Wm}^{-1}\text{K}^{-1}$ are the thermal conductivities of quartz, soil minerals
 218 other than quartz, water and SOM, respectively. The volumetric fraction of soil minerals other
 219 than quartz is defined as:

220 $f_{other} = 1 - f_q - \theta_{sat} - f_{SOM}$
 221 with $f_q = Q \times (1 - \theta_{sat})$ (11)
 222

223 2.6. Reverse modelling 224

225 The λ_{sat} values are retrieved through reverse modelling using the λ model described above (Eqs.
 226 (7)-(11)). The λ model is used to produce simulations of λ at the same soil moisture conditions as
 227 those encountered for the λ values derived from observations in Sect. 2.4. For a given station, a
 228 set of 401 simulations is produced for λ_{sat} ranging from $0 \text{ Wm}^{-1}\text{K}^{-1}$ to $4 \text{ Wm}^{-1}\text{K}^{-1}$, with a
 229 resolution of $0.01 \text{ Wm}^{-1}\text{K}^{-1}$. The λ_{sat} retrieval corresponds to the λ simulation presenting the
 230 lowest root mean square difference (RMSD) value with respect to the λ observations. Only λ
 231 observations for S_d values higher than 0.4 are used because in dry conditions: (1) conduction is
 232 not the only mechanism for heat exchange in soils, as the convective water vapour flux may
 233 become significant (Schelde et al., 1998, Parlange et al. 1998), (2) the K_e functions found in the
 234 literature display more variability, (3) the λ_{sat} retrievals are more sensitive to uncertainties in λ
 235 observations. The threshold value of $S_d = 0.4$ results from a compromise between the need of

236 limiting the influence of convection, of the shape of the K_e function on the retrieved values of
237 λ_{sat} , and of using as many observations as possible in the retrieval process. Moreover, the data
238 filtering technique to limit the impact of soil heterogeneities, described in Supplement 2, is used
239 to select valid λ observations.

240 Finally, the f_q value is derived from the retrieved λ_{sat} solving Eq. (10).

241

242 2.7. Scores

243

244 Pedotransfer functions for quartz and λ_{sat} are evaluated using the following scores:

- 245 • the Pearson correlation coefficient (r), and the squared correlation coefficient (r^2) is used
246 to assess the fraction of explained variance,
- 247 • the RMSD,
- 248 • the Mean Absolute Error (MAE), i.e. the mean of absolute differences,
- 249 • the mean bias, i.e. the mean of differences.

250 In order to test the predictive and generalization power of the pedotransfer regression equations, a
251 simple bootstrapping resampling technique is used. It consists in calculating a new estimate of f_q
252 for each soil using the pedotransfer function obtained without using this specific soil. Gathering
253 these new f_q estimates, one can calculate new scores with respect to the retrieved f_q values. Also,
254 this method provides a range of possible values of the coefficients of the pedotransfer function
255 and permits assessing the influence of a given f_q retrieval on the final result.

256

256 **3. Results**

257
258
259 3.1. λ_{sat} and f_{q} retrievals
260
261
262 Retrievals of λ_{sat} and f_{q} could be obtained for 14 soils. Figure 3 shows retrieved and modelled λ
263 values vs. the observed degree of saturation of the soil, at a depth of 0.10 m, for contrasting
264 retrieved values of λ_{sat} , from high to low λ_{sat} values (2.80, 1.96, 1.52, and 1.26 $\text{Wm}^{-1}\text{K}^{-1}$) at the
265 SBR, MNT, MTM, and PRD stations, respectively.

266 All the obtained λ_{sat} and f_{q} retrievals are listed in Table 2, together with the λ RMSD values and
267 the number of selected λ observations. For three soils (CRD, MZN, and VLV), the reverse
268 modelling technique described in Sect. 2.6 could not be applied as not enough λ observations
269 could be obtained for S_{d} values higher than 0.4. For four soils (NBN, PZN, BRZ, and MJN), all
270 the λ retrievals were filtered out as the obtained values were influenced by heterogeneities in soil
271 density (see Supplement 2). For the other 14 soils, λ_{sat} and f_{q} retrievals were obtained using a
272 subset of 20 λ retrievals per soil, at most, corresponding to the soil temperature data presenting
273 the lowest vertical gradient close to the soil surface (Supplement 2).

274
275 3.2 Pedotransfer functions for quartz
276

277 The f_{q} retrievals can be used to assess the possibility to estimate f_{q} using other soil characteristics,
278 which can be easily measured. Another issue is whether volumetric or gravimetric fraction of
279 quartz should be used. Figure 4 presents the fraction of variance (r^2) of Q and f_{q} explained by
280 various indicators. A key result is that f_{q} is systematically better correlated to soil characteristics
281 than Q . More than 60 % of the variance of f_{q} can be explained using indicators based on the sand

282 fraction (either f_{sand} or m_{sand}). The use of other soil mineral fractions does not give good
283 correlations, even when they are associated to the sand fraction as shown by Fig. 4. For example,
284 the f_{gravel} and $f_{\text{gravel}+f_{\text{sand}}}$ indicators present low r^2 values of 0.04 and 0.24, respectively.

285 The f_q values cannot be derived directly from the indicators as illustrated by Fig. 5: assuming $f_q =$
286 f_{sand} tends to markedly underestimate λ_{sat} . Therefore, more elaborate pedotransfer equations are
287 needed. They can be derived from the best indicators, using them as predictors of f_q . The
288 modelled f_q is written as:

$$289 \quad f_{qMOD} = a_0 + a_1 \times P$$

$$290 \quad \text{and } f_{qMOD} \leq 1 - \theta_{\text{sat}} - f_{SOM} \quad (12)$$

291 where P represents the predictor of f_q .

292 The a_0 and a_1 coefficients are given in Table 3 for four pedotransfer functions based on the best
293 predictors of f_q . The pedotransfer functions are illustrated in Fig. 6. The scores are displayed in
294 Table 4. The bootstrapping indicates that the SBR sandy soil has the largest individual impact on
295 the obtained regression coefficients. This is why the scores without SBR are also presented in
296 Table 4.

297 For the m_{sand} predictor, a r^2 value of 0.56 is obtained without SBR, against a value of 0.67 when
298 all the 14 soils are considered. An alternative to this m_{sand} pedotransfer function consists in
299 considering only m_{sand} values smaller than 0.6 kg kg^{-1} in the regression, thus excluding the SBR
300 soil. The corresponding predictor is called m_{sand}^* . In this configuration, the sensitivity of f_q to
301 m_{sand} is much increased (with $a_1 = 0.944$, against $a_1 = 0.572$ with SBR). For SBR, f_q is
302 overestimated by the m_{sand}^* equation but this is corrected by the f_{qMOD} limitation of Eq. (12), and
303 in the end a better r^2 score is obtained when the 14 soils are considered ($r^2 = 0.74$).

304 Values of r^2 larger than 0.7 are obtained for two predictors of f_q : $m_{\text{sand}}/m_{\text{SOM}}$ and m_{sand}^* . A value
 305 of $r^2 = 0.65$ is obtained for $1 - \theta_{\text{sat}} - f_{\text{sand}}$ (the fraction of soil solids other than sand). The
 306 $m_{\text{sand}}/m_{\text{SOM}}$ predictor presents the best r^2 and RMSD scores in all the configurations (regression,
 307 bootstrap, and regression without SBR). Another characteristic of the $m_{\text{sand}}/m_{\text{SOM}}$ pedotransfer
 308 function is that the confidence interval for the a_0 and a_1 coefficients derived from bootstrapping is
 309 narrower than for the other pedotransfer functions (Table 3), indicating a more robust relationship
 310 of f_q with $m_{\text{sand}}/m_{\text{SOM}}$ than with other predictors. Modelled values of λ_{sat} (λ_{satMOD}) can be derived
 311 from $f_{q\text{MOD}}$ using Eq. (10) together with θ_{sat} observations. The λ_{satMOD} r^2 , RMSD, and mean bias
 312 scores are given in Table 5. Again, the best scores are obtained using the $m_{\text{sand}}/m_{\text{SOM}}$ predictor of
 313 f_q , with r^2 , RMSD, and mean bias values of 0.86, 0.14 $\text{Wm}^{-1}\text{K}^{-1}$, and +0.01 $\text{Wm}^{-1}\text{K}^{-1}$, respectively
 314 (Fig. 7).

315 Finally, we investigated the possibility of estimating θ_{sat} from the soil characteristics listed in
 316 Table 1 and of deriving a statistical model for θ_{sat} (θ_{satMOD}). We found the following statistical
 317 relationship between θ_{satMOD} , m_{clay} , m_{silt} , and m_{SOM} :

$$318 \quad \theta_{\text{satMOD}} = 0.456 - 0.0735 \frac{m_{\text{clay}}}{m_{\text{silt}}} + 2.238 m_{\text{SOM}} \quad (13)$$

319 ($r^2 = 0.48$, F-test p -value = 0.0027, RMSD=0.036 m^3m^{-3}).

320 Volumetric fractions of soil components need to be consistent with θ_{satMOD} and can be calculated
 321 using the modelled bulk density values derived from θ_{satMOD} using Eq. (1).

322 Equations (10) to (13) constitute an empirical end-to-end model of λ_{sat} . Table 5 shows that using
 323 θ_{satMOD} (Eqs. (13)) instead of the θ_{sat} observations has little impact on the λ_{satMOD} scores.

324

325

325
326
327
328
329
330
331
332
333
334
335
336
337
338
339
340
341
342
343
344
345
346
347

3.3. Impact of gravels and SOM on λ_{sat}

Gravels and SOM are often neglected in soil thermal conductivity models used in LSMs. The Eqs. (10)-(13) empirical model obtained in Sect. 3.2 permits the assessment of the impact of f_{gravel} and f_{SOM} on λ_{sat} . Table 5 shows the impact on λ_{satMOD} scores of imposing a null value of f_{gravel} and a small value of f_{SOM} to all the soils. The combination of these assumptions is evaluated, also.

Imposing $f_{\text{SOM}} = 0.013 \text{ m}^3 \text{ m}^{-3}$ (the smallest f_{SOM} value, observed for CBR) has a limited impact on the scores, except for the $m_{\text{sand}}/m_{\text{SOM}}$ pedotransfer function. In this case, λ_{sat} is overestimated by $+0.20 \text{ Wm}^{-1}\text{K}^{-1}$, and r^2 drops to 0.57.

Neglecting gravels ($f_{\text{gravel}} = 0 \text{ m}^3 \text{ m}^{-3}$) also has a limited impact but triggers the underestimation (overestimation) of λ_{sat} for the $m_{\text{sand}}/m_{\text{SOM}}$ (m_{sand}^*) pedotransfer function, by $-0.12 \text{ Wm}^{-1}\text{K}^{-1}$ ($+0.11 \text{ Wm}^{-1}\text{K}^{-1}$).

On the other hand, it appears that combining these assumptions has a marked impact on all the pedotransfer functions. Neglecting gravels and imposing $f_{\text{SOM}} = 0.013 \text{ m}^3 \text{ m}^{-3}$ has a major impact on λ_{sat} : the modelled λ_{sat} is overestimated by all the pedotransfer functions (with a mean bias ranging from $+0.16 \text{ Wm}^{-1}\text{K}^{-1}$ to $+0.24 \text{ Wm}^{-1}\text{K}^{-1}$) and r^2 is markedly smaller, especially for the m_{sand} and m_{sand}^* pedotransfer functions. These results are illustrated in Fig. 8 in the case of the m_{sand}^* pedotransfer function. Figure 8 also shows that using the θ_{sat} observations instead of θ_{satMOD} (Eq. (13)) has little impact on λ_{satMOD} (Sect. 3.2) but tends to enhance the impact of neglecting gravels. A similar result is found with the m_{sand} pedotransfer function (not shown).

348

349 **4. Discussion**

350

351 4.1. Sources of uncertainties in heat capacity estimates

352

353

354 In this study, the de Vries (1963) mixing model is applied to estimate soil volumetric heat
355 capacity, and a fixed value of $2.0 \times 10^6 \text{ J m}^{-3} \text{ K}^{-1}$ is used for soil minerals (Eq. (6)). Soil-specific
356 values for C_{hmin} may be more appropriate than using a constant standard value. For example,
357 Tarara and Ham (1997) used a value of $1.92 \times 10^6 \text{ J m}^{-3} \text{ K}^{-1}$. However, we did not measure this
358 quantity and we were not able to find such values in the literature.

359 We investigated the sensitivity of our results to these uncertainties, considering the following
360 minimum and maximum C_{hmin} values: $C_{\text{hmin}} = 1.92 \times 10^6 \text{ J m}^{-3} \text{ K}^{-1}$ and $C_{\text{hmin}} = 2.08 \times 10^6 \text{ J m}^{-3}$
361 K^{-1} . The impact of changes in C_{hmin} on the retrieved values of λ_{sat} and f_q is presented in Fig. 9. On
362 average, a change of $+ (-) 0.08 \times 10^6 \text{ J m}^{-3} \text{ K}^{-1}$ in C_{hmin} triggers a change in λ_{sat} and f_q of $+ 1.7 \%$
363 $(- 1.8 \%)$ and $+ 4.8 \%$ $(- 7.0 \%)$, respectively.

364 The impact of changes in C_{hmin} on the regression coefficients of the pedotransfer functions is
365 presented in Table 3 (last column). The impact is very small, except for the a_1 coefficient of the
366 m_{sand}^* pedotransfer function. However, even in this case, the impact of C_{hmin} on the a_1 coefficient
367 is much lower than the confidence interval given by the bootstrapping, indicating that the
368 relatively small number of soils considered in this study (as in other studies, e.g. Lu et al. (2007))
369 is a larger source of uncertainty.

370 Moreover, uncertainties in the f_{clay} , f_{silt} , f_{gravel} , or f_{SOM} fractions may be caused by (1) the natural
371 heterogeneity of soil properties, (2) the living root biomass, (3) stones that may not be accounted
372 for in the gravel fraction.

373 In particular, during the installation of the probes, it was observed that stones are present at some
374 stations. Stones are not evenly distributed in the soil, and it is not possible to investigate whether
375 the soil area where the temperature probes were inserted contains stones as it must be left
376 unperturbed.

377 The grasslands considered in this study are not intensively managed. They consist of set-aside
378 fields cut once or twice a year. Calvet et al. (1999) gave an estimate of 0.160 kg m^{-2} for the root
379 dry matter content of such soils for a site in southwestern France, with most roots contained in
380 the 0.25m top soil layer. This represents a gravimetric fraction of organic matter smaller than
381 $0.0005 \text{ kg kg}^{-1}$, i.e. less than 4% of the lowest m_{SOM} values observed in this study (0.013 kg kg^{-1})
382 or less than 5% of f_{SOM} values. We checked that increasing f_{SOM} values by 5% has negligible
383 impact on heat capacity and on the λ retrievals.

384

385

386 4.3. Applicability of the new λ_{sat} model to other soil types

387

388 The λ_{sat} values found in this study are consistent with values reported by other authors. In this
389 study, λ_{sat} values ranging between $1.26 \text{ Wm}^{-1}\text{K}^{-1}$ and $2.80 \text{ Wm}^{-1}\text{K}^{-1}$ are found (Table 2).
390 Tarnawski et al. (2011) gave λ_{sat} values ranging between $2.5 \text{ Wm}^{-1}\text{K}^{-1}$ and $3.5 \text{ Wm}^{-1}\text{K}^{-1}$ for
391 standard sands. Lu et al. (2007) gave λ_{sat} values ranging between $1.33 \text{ Wm}^{-1}\text{K}^{-1}$ and 2.2
392 $\text{Wm}^{-1}\text{K}^{-1}$.

393 A key component of the λ_{sat} model is the pedotransfer function for quartz (Eq. (12)). The f_q
394 pedotransfer functions proposed in this study are based on basic soil characteristics. The current
395 global soil digital maps provide information about SOM, gravels and bulk density (Nachtergaele
396 et al., 2012). Therefore, using Eq. (1) and Eqs. (6)-(12) at large scale is possible, and porosity can
397 be derived from Eq. (1). On the other hand, the suggested f_q pedotransfer functions are obtained
398 for temperate grassland soils containing a rather large amount of organic matter, and are valid for
399 $m_{\text{sand}}/m_{\text{SOM}}$ ratio values lower than 40 (Table 2). These equations should be evaluated for other
400 regions. In particular, hematite has to be considered together with quartz for tropical soils.
401 Moreover, while the pedotransfer function we get for θ_{sat} (Eq. (13)) is valid for the specific sites
402 considered in this study and is used to conduct the sensitivity study of Sect. 3.3, Eq. (13) cannot
403 be used to predict porosity in other regions.

404 In order to assess the applicability of the pedotransfer function for quartz obtained in this study,
405 we used the independent data from Lu et al. (2007) and Tarnawski et al. (2009), for ten Chinese
406 soils (see Supplement 3 and Table S3.1). These soils consist of reassembled sieved soil samples
407 and contain no gravel, while our data concern undisturbed soils. Moreover, most of these soils
408 contain very little organic matter and the $m_{\text{sand}}/m_{\text{SOM}}$ ratio can be much larger than the $m_{\text{sand}}/m_{\text{SOM}}$
409 values measured at our grassland sites. For the 14 French soils used to determine pedotransfer
410 functions for quartz, the $m_{\text{sand}}/m_{\text{SOM}}$ ratio ranges from 3.7 to 37.2 (Table 2). Only three soils of Lu
411 et al. (2007) present such low values of $m_{\text{sand}}/m_{\text{SOM}}$. The other seven soils of Lu et al. (2007)
412 present $m_{\text{sand}}/m_{\text{SOM}}$ values ranging from 48 to 1328 (see Table S3.1).

413 We used λ_{sat} experimental values derived from Table 3 in Tarnawski et al. (2009) to calculate Q
414 and f_q for the ten Lu et al. (2007) soils. Figure 10 shows the statistical relationship between these
415 quantities and m_{sand} . Very good correlations of Q and f_q with m_{sand} are observed, with r^2 values of

416 0.72 and 0.83, respectively. This is consistent with our finding that f_q is systematically better
417 correlated to soil characteristics than Q (Sect. 3.2).

418 The pedotransfer functions derived from French soils tend to overestimate f_q for the Lu et al.
419 (2007) soils, especially for the seven soils presenting $m_{\text{sand}}/m_{\text{SOM}}$ values larger than 40. Note that
420 Lu et al. (2007) obtained a similar result for coarse-textured soils with their model, which
421 assumed $Q = m_{\text{sand}}$. For the three other soils, presenting $m_{\text{sand}}/m_{\text{SOM}}$ values smaller than 40, f_q
422 MAE values are given in Table 4. The best MAE score ($0.071 \text{ m}^3 \text{ m}^{-3}$) is obtained for the m_{sand}^*
423 predictor of f_q .

424 These results are illustrated by Fig. 11 for the m_{sand} predictor of f_q . Figure 11 also shows the f_q
425 and λ_{sat} estimates obtained using specific coefficients in Eq. (12), based on the seven Lu et al.
426 (2007) soils presenting $m_{\text{sand}}/m_{\text{SOM}}$ values larger than 40. These coefficients are given together
427 with the scores in Table 6. Table 6 also present these values for other predictors of f_q . It appears
428 that m_{sand} gives the best scores. The contrasting coefficient values between Table 6 and Table 3
429 (Chinese and French soils, respectively) illustrate the variability of the coefficients of
430 pedotransfer functions from one soil category to another, and the $m_{\text{sand}}/m_{\text{SOM}}$ ratio seems to be a
431 good indicator of the validity of a given pedotransfer function.

432 On the other hand, the $m_{\text{sand}}/m_{\text{SOM}}$ ratio is not a good predictor of f_q for the Lu et al. (2007) soils
433 presenting $m_{\text{sand}}/m_{\text{SOM}}$ values larger than 40, and r^2 presents a small value of 0.40 (Table 6). This
434 can be explained by the very large range of $m_{\text{sand}}/m_{\text{SOM}}$ values for these soils (see Table S3.1).
435 Using $\ln(m_{\text{sand}}/m_{\text{SOM}})$ instead of $m_{\text{sand}}/m_{\text{SOM}}$ is a way to obtain a predictor linearly correlated to f_q .
436 This is shown by Fig. 12 for the ten Lu et al. (2007) soils: the correlation is increased to a large
437 extent ($r^2 = 0.60$).

438

439

440 4.4. Can m_{sand} -based f_q pedotransfer functions be used across soil types ?

441 Given the results presented in Tables 3, 4, and 6, it can be concluded that m_{sand} is the best
442 predictor of f_q across mineral soil types. The $m_{\text{sand}}/m_{\text{SOM}}$ predictor is relevant for the mineral soils
443 containing the largest amount of organic matter.

444 The results presented in this study suggest that the $m_{\text{sand}}/m_{\text{SOM}}$ ratio can be used to differentiate
445 temperate grassland soils containing a rather large amount of organic matter ($3.7 < m_{\text{sand}}/m_{\text{SOM}} <$
446 40) from soils containing less organic matter ($m_{\text{sand}}/m_{\text{SOM}} > 40$). The m_{sand} predictor can be used
447 in both cases, with the following a_0 and a_1 coefficient values in Eq. (12): 0.15 and 0.572 for
448 $m_{\text{sand}}/m_{\text{SOM}}$ ranging between 3.7 and 40 (Table 3), and 0.04 and 0.386 for $m_{\text{sand}}/m_{\text{SOM}} > 40$ (Table
449 6), respectively.

450 Although the $m_{\text{sand}}/m_{\text{SOM}}$ predictor gives the best r^2 scores for the 14 grassland soils considered in
451 this study, it seems more difficult to apply this predictor to other soils, as shown by the high
452 MAE score (MAE = $0.135 \text{ m}^3 \text{ m}^{-3}$) for the corresponding Lu et al. (2007) soils in Table 4.
453 Moreover, the scores are very sensitive to errors in the estimation of m_{SOM} as shown by Table 5.

454 Although the m_{sand}^* predictor gives slightly better scores than m_{sand} (Table 4), the a_1 coefficient in
455 more sensitive to errors in C_{hmin} (Table 3), and the bootstrapping reveals large uncertainties in a_0
456 and a_1 values.

457

458

459

460

461
462 4.5. Prospects for using soil temperature profiles
463
464 Using standard soil moisture and soil temperature observations is a way to investigate soil
465 thermal properties over a large variety of soils, as the access to such data is facilitated by online
466 databases (Dorigo et al., 2013).
467 A limitation of the data used in this study, however, is that soil temperature observations (T_i) are
468 recorded with a resolution of $\Delta T_i = 0.1$ °C only (see Sect. 2.1). This low resolution affects the
469 accuracy of the soil thermal diffusivity estimates. In order to limit the impact of this effect, a data
470 filtering technique is used (see Supplement 4) and D_h is retrieved with a precision of 18 %.
471 It can be noticed that if T_i data were recorded with a resolution of 0.03 °C (which corresponds to
472 the typical uncertainty of PT100 probes), D_h could be retrieved with a precision of about 5 % in
473 the conditions of Eq. (S4.3). Therefore, one may recommend to revise the current practise of
474 most observation networks consisting in recording soil temperature with a resolution of 0.1 °C
475 only. More precision in the λ estimates would permit investigating other processes of heat
476 transfer in the soil such as those related to water transport (Rutten, 2015).

477
478
479

479 **5. Conclusions**

480

481 An attempt was made to use routine soil temperature and soil moisture observations of a network
482 of automatic weather stations to retrieve instantaneous values of the soil thermal conductivity at
483 a depth of 0.10 m. The data from the SMOSMANIA network, in southern France, are used. First,
484 the thermal diffusivity is derived from consecutive measurements of the soil temperature. The λ
485 values are then derived from the thermal diffusivity retrievals and from the volumetric heat
486 capacity calculated using measured soil properties. The relationship between the λ estimates and
487 the measured soil moisture at a depth of 0.10 m permits the retrieval of λ_{sat} for 14 stations. The
488 Lu et al. (2007) empirical λ model is then used to retrieve the quartz volumetric content by
489 reverse modelling. A number of pedotransfer functions is proposed for volumetric fraction of
490 quartz, for the considered region in France. For the grassland soils examined in this study, the
491 ratio of sand to SOM fractions is the best predictor of f_q . A sensitivity study shows that omitting
492 gravels and the SOM information has a major impact on λ_{sat} . Eventually, an error propagation
493 analysis and a comparison with independent λ_{sat} data from Lu et al. (2007) show that the
494 gravimetric fraction of sand within soil solids, including gravels and SOM, is a good predictor of
495 the volumetric fraction of quartz when a larger variety of soil types is considered.

496

497 **Acknowledgements**

498 We thank Dr. Xinhua Xiao (NC State University Soil Physics, Raleigh, USA) and Dr. Tusheng
499 Ren (China Agricultural University, Beijing, China) for their review of the manuscript and for
500 their fruitful comments. We thank Dr. Aaron Boone (CNRM, Toulouse, France) for his helpful
501 comments. We thank our Meteo-France colleagues for their support in collecting and archiving

502 the SMOSMANIA data: Catherine Bienaimé, Marc Bailleul, Laurent Brunier, Anna Chaumont,
503 Jacques Couzinier, Mathieu Créau, Philippe Gillodes, Sandrine Girres, Michel Gouverneur,
504 Maryvonne Kerdoncuff, Matthieu Lacan, Pierre Lantuejoul, Dominique Paulais, Fabienne Simon,
505 Dominique Simonpietri, Marie-Hélène Théron, Marie Yardin.
506

506 **References**

- 507
- 508 Abu-Hamdeh, N. H., and Reeder, R. C.: Soil thermal conductivity: effects of density, moisture,
509 salt concentration, and organic matter, *Soil Sci. Soc. Am. J.*, 64, 1285–1290, 2000.
- 510 Albergel, C., Rüdiger, C., Pellarin, T., Calvet, J.-C., Fritz, N., Froissard, F., Suquia, D., Petitpa,
511 A., Piguet, B., and Martin, E.: From near-surface to root-zone soil moisture using an
512 exponential filter: an assessment of the method based on in-situ observations and model
513 simulations, *Hydrol. Earth Syst. Sci.*, 12, 1323–1337, 2008.
- 514 Albergel, C., Calvet, J.-C., de Rosnay, P., Balsamo, G., Wagner, W., Hasenauer, S., Naeimi, V.,
515 Martin, E., Bazile, E., Bouyssel, F., and Mahfouf, J.-F.: Cross-evaluation of modelled and
516 remotely sensed surface soil moisture with in situ data in southwestern France, *Hydrol. Earth
517 Syst. Sci.*, 14, 2177–2191, doi:10.5194/hess-14-2177-2010, 2010.
- 518 Bristow, K. L., Kluitenberg, G. J., and Horton R.: Measurement of soil thermal properties with a
519 dual-probe heat-pulse technique, *Soil Sci. Soc. Am. J.*, 58, 1288–1294,
520 doi:10.2136/sssaj1994.03615995005800050002x, 1994.
- 521 Bristow, K. L.: Measurement of thermal properties and water content of unsaturated sandy soil
522 using dual-probe heat-pulse probes, *Agr. Forest Meteorol.*, 89, 75-84, 1998.
- 523 Calvet, J.-C., Bessemoulin, P., Noilhan, J., Berne, C., Braud, I., Courault, D., Fritz, N., Gonzalez-
524 Sosa, E., Goutorbe, J.-P., Haverkamp, R., Jaubert, G., Kergoat, L., Lachaud, G., Laurent, J.-
525 P., Mordelet, P., Olioso, A., Péris, P., Roujean, J.-L., Thony, J.-L., Tosca, C., Vauclin, M.,
526 Vignes, D.: MUREX: a land-surface field experiment to study the annual cycle of the energy
527 and water budgets, *Ann. Geophys.*, 17, 838-854, 1999.
- 528 Calvet, J.-C., Fritz, N., Froissard, F., Suquia, D., Petitpa, A., and Piguet, B.: In situ soil moisture
529 observations for the CAL/VAL of SMOS: the SMOSMANIA network, *International*

530 Geoscience and Remote Sensing Symposium, IGARSS, Barcelona, Spain, 23–28 July 2007,
531 1196–1199, doi:10.1109/IGARSS.2007.4423019, 2007.

532 Chen, Y. Y., Yang, K., Tang, W., Qin, J., and Zhao, L.: Parameterizing soil organic carbon's
533 impacts on soil porosity and thermal parameters for Eastern Tibet grasslands, *Sci. China*
534 *Earth Sci.*, 55 (6), 1001–1011, doi:10.1007/s11430-012-4433-0, 2012.

535 Côté, J. and Konrad, J.-M.: A generalized thermal conductivity model for soils and construction
536 materials, *Can. Geotech. J.*, 42, 443:458, doi:10.1139/T04-106, 2005.

537 de Vries, D. A.: Thermal properties of soils, in W.R. Van Wijk (ed.), *Physics of plant*
538 *environment*, pp. 210–235, North-Holland Publ. Co., Amsterdam, 1963.

539 Dorigo, W. A., Wagner, W., Hohensinn, R., Hahn, S., Paulik, C., Xaver, A., Gruber, A., Drusch, M.,
540 Mecklenburg, S., van Oevelen, P., Robock, A., and Jackson, T.: The International Soil
541 Moisture Network: a data hosting facility for global in situ soil moisture measurements,
542 *Hydrol. Earth Syst. Sci.*, 15, 1675–1698, doi:10.5194/hess-15-1675-2011, 2011.

543 Draper, C., Mahfouf, J.-F., Calvet, J.-C., Martin, E., and Wagner, W.: Assimilation of ASCAT
544 near-surface soil moisture into the SIM hydrological model over France, *Hydrol. Earth Syst.*
545 *Sci.*, 15, 3829–3841, doi:10.5194/hess-15-3829-2011, 2011.

546 Johansen, O.: Thermal conductivity of soils. Ph.D. thesis, University of Trondheim, 236 pp.,
547 Available from Universitetsbiblioteket i Trondheim, Høgskoleringen 1, 7034 Trondheim,
548 Norway, a translation is available at: <http://www.dtic.mil/dtic/tr/fulltext/u2/a044002.pdf> (last
549 access January 2016), 1975.

550 Lu, S., Ren, T., Gong, Y., and Horton, R.: An improved model for predicting soil thermal
551 conductivity from water content at room temperature, *Soil Sci. Soc. Am. J.*, 71, 8-14,
552 doi:10.2136/sssaj2006.0041, 2007.

553 Nachtergaele, F., van Velthuize, H., Verelst, L., Wiberg, D., Batjes, N., Dijkshoorn, K., van
554 Engelen, V., Fischer, G., Jones, A., Montanarella, L., Petri, M., Prieler, S., Teixeira, E., and

555 Shi, X.: Harmonized World Soil Database, Version 1.2, FAO/IIASA/ISRIC/ISS-CAS/JRC,
556 FAO, Rome, Italy and IIASA, Laxenburg, Austria, available at:
557 [http://webarchive.iiasa.ac.at/Research/LUC/External-World-soil-
558 database/HWSD_Documentation.pdf](http://webarchive.iiasa.ac.at/Research/LUC/External-World-soil-
558 database/HWSD_Documentation.pdf) (last access January 2016), 2012.

559 Parlange, M. B., Cahill, A. T., Nielsen, D. R., Hopmans, J. W., and Wendroth, O.: Review of
560 heat and water movement in field soils, *Soil Till. Res.*, 47, 5-10, 1998.

561 Parrens, M., Zakharova, E., Lafont, S., Calvet, J.-C., Kerr, Y., Wagner, W., and Wigneron, J.-P.:
562 Comparing soil moisture retrievals from SMOS and ASCAT over France, *Hydrol. Earth Syst.*
563 *Sci.*, 16, 423–440, doi:10.5194/hess-16-423-2012, 2012.

564 Peters-Lidard, C.D., Blackburn, E., Liang, X., and Wood, E.F.: The effect of soil thermal
565 conductivity parameterization on surface energy fluxes and temperatures, *J. Atmos. Sci.*, 55,
566 1209–1224, 1998.

567 Rutten, M. M.: Moisture in the topsoil: From large-scale observations to small-scale process
568 understanding, PhD Thesis, Delft university of Technology, doi:10.4233/uuid:89e13a16-
569 b456-4692-92f0-7a40ada82451, available at:
570 <http://repository.tudelft.nl/view/ir/uuid:89e13a16-b456-4692-92f0-7a40ada82451/> (last
571 access: January 2016), 2015.

572

573 Schelde, K., Thomsen, A., Heidmann, T., Schjonning, P., and Jansson, P.-E.: Diurnal fluctuations
574 of water and heat flows in a bare soil, *Water Resour. Res.*, 34, 11, 2919-2929, 1998.

575 Schönenberger, J., Momose, T., Wagner, B., Leong, W. H., and Tarnawski, V. R.: Canadian field
576 soils I. Mineral composition by XRD/XRF measurements, *Int. J. Thermophys.*, 33, 342–362,
577 doi:10.1007/s10765-011-1142-4, 2012.

578 Tarara, J.M., and J.M. Ham: Measuring soil water content in the laboratory and field with dual-
579 probe heat-capacity sensors, *Agron. J.*, 89, 535–542, 1997.

580 Tarnawski, V. R., McCombie, M. L., Leong, W. H., Wagner, B., Momose, T., and
581 Schöenberger J.: Canadian field soils II. Modeling of quartz occurrence, *Int. J.*
582 *Thermophys.*, 33, 843–863, doi:10.1007/s10765-012-1184-2, 2012.

583 Tarnawski, V. R., Momose, T., and Leong, W. H.: Assessing the impact of quartz content on the
584 prediction of soil thermal conductivity, *Géotechnique*, 59, 4, 331–338, doi:
585 10.1680/geot.2009.59.4.331, 2009.

586 Yang, K., Koike, T., Ye, B., and Bastidas, L.: Inverse analysis of the role of soil vertical
587 heterogeneity in controlling surface soil state and energy partition, *J. Geophys. Res.*, 110,
588 D08101, 15 pp., doi:10.1029/2004JD005500, 2005.

589 Zhang, X., Heitman, J., Horton, R., and Ren, T.: Measuring near-surface soil thermal properties
590 with the heat-pulse method: correction of ambient temperature and soil–air interface effects,
591 *Soil Sci. Soc. Am. J.*, 78, 1575–1583, doi:10.2136/sssaj2014.01.0014, 2014.

592

592 **Table 1** – Soil characteristics at 10 cm for the 21 stations of the SMOSMANIA network.
593 Porosity values are derived from Eq. (1). Solid fraction values higher than 0.3 are in bold. The
594 stations are listed from West to East (from top to bottom). ρ_d , θ_{sat} , f , and m , stand for soil bulk
595 density, porosity, volumetric fractions, and gravimetric fractions, respectively.
596

Soil	ρ_d (kg m ⁻³)	θ_{sat} (m ³ m ⁻³)	f_{sand} (m ³ m ⁻³)	f_{clay} (m ³ m ⁻³)	f_{silt} (m ³ m ⁻³)	f_{gravel} (m ³ m ⁻³)	f_{SOM} (m ³ m ⁻³)	m_{sand} (kg kg ⁻¹)	m_{clay} (kg kg ⁻¹)	m_{silt} (kg kg ⁻¹)	m_{gravel} (kg kg ⁻¹)	m_{SOM} (kg kg ⁻¹)
SBR	1680	0.352	0.576	0.026	0.013	0.002	0.032	0.911	0.041	0.020	0.003	0.024
URG	1365	0.474	0.076	0.078	0.341	0.005	0.025	0.149	0.153	0.665	0.009	0.024
CRD	1435	0.438	0.457	0.027	0.033	0.000	0.045	0.848	0.051	0.060	0.000	0.041
PRG	1476	0.431	0.051	0.138	0.138	0.214	0.028	0.092	0.250	0.248	0.385	0.025
CDM	1522	0.413	0.073	0.241	0.231	0.012	0.030	0.128	0.422	0.404	0.020	0.026
LHS	1500	0.416	0.102	0.202	0.189	0.051	0.039	0.181	0.359	0.335	0.091	0.034
SVN	1453	0.445	0.127	0.073	0.176	0.162	0.017	0.233	0.133	0.322	0.296	0.015
MNT	1444	0.447	0.135	0.066	0.230	0.102	0.020	0.248	0.121	0.424	0.188	0.018
SFL	1533	0.413	0.127	0.071	0.118	0.250	0.021	0.221	0.123	0.205	0.434	0.018
MTM	1540	0.405	0.110	0.081	0.076	0.297	0.032	0.189	0.140	0.131	0.512	0.027
LZC	1498	0.429	0.129	0.066	0.068	0.292	0.015	0.229	0.117	0.121	0.519	0.013
NBN	1545	0.401	0.063	0.135	0.075	0.290	0.035	0.109	0.232	0.130	0.499	0.030
PZN	1311	0.495	0.222	0.074	0.131	0.054	0.023	0.450	0.151	0.266	0.111	0.023
PRD	1317	0.494	0.038	0.052	0.069	0.326	0.021	0.076	0.105	0.139	0.659	0.021
LGC	1496	0.428	0.253	0.044	0.042	0.214	0.019	0.451	0.078	0.074	0.380	0.017
MZN	1104	0.560	0.212	0.037	0.045	0.097	0.049	0.510	0.089	0.109	0.234	0.057
VLV	1274	0.506	0.294	0.054	0.086	0.031	0.029	0.614	0.112	0.179	0.064	0.030
BRN	1630	0.379	0.105	0.009	0.016	0.474	0.016	0.171	0.015	0.027	0.774	0.013
MJN	1276	0.506	0.064	0.029	0.056	0.317	0.028	0.133	0.060	0.118	0.661	0.029
BRZ	1280	0.508	0.097	0.074	0.109	0.190	0.020	0.202	0.154	0.228	0.396	0.021
CBR	1310	0.501	0.120	0.057	0.068	0.241	0.013	0.243	0.116	0.139	0.489	0.013

597
598

598 **Table 2** – Thermal properties of 14 grassland soils in southern France: λ_{sat} , f_q and Q retrievals
599 using the λ model (Eqs. (7)-(9) and Eq. (10), respectively) for degree of saturation values higher
600 than 0.4, together with the minimized RMSD between the simulated and observed λ values, and
601 the number of used λ observations (n). The soils are sorted from the largest to the smallest ratio
602 of m_{sand} to m_{SOM} .
603

Soil	λ_{sat} ($\text{Wm}^{-1}\text{K}^{-1}$)	RMSD ($\text{Wm}^{-1}\text{K}^{-1}$)	n	f_q (m^3m^{-3})	Q (kg kg^{-1})	$\frac{m_{\text{sand}}}{m_{\text{SOM}}}$
SBR	2.80	0.255	6	0.62	0.96	37.2
LGC	2.07	0.311	20	0.44	0.77	26.6
CBR	1.92	0.156	20	0.44	0.88	18.4
LZC	1.71	0.107	20	0.29	0.51	17.3
SVN	1.78	0.163	20	0.34	0.61	15.4
MNT	1.96	0.058	20	0.42	0.76	13.8
BRN	1.71	0.131	20	0.25	0.40	13.5
SFL	1.57	0.134	20	0.22	0.37	12.5
MTM	1.52	0.095	20	0.21	0.35	7.0
URG	1.37	0.066	20	0.05	0.10	6.2
LHS	1.57	0.136	20	0.26	0.45	5.3
CDM	1.82	0.086	20	0.26	0.44	5.0
PRG	1.65	0.086	20	0.18	0.32	3.7
PRD	1.26	0.176	20	0.14	0.28	3.7

604
605
606
607
608
609

609 **Table 3** – Coefficients of four pedotransfer functions of f_q for 14 soils of this study, together
 610 with indicators of the coefficient uncertainty, derived by bootstrapping and by perturbing the
 611 volumetric heat capacity of soil minerals (C_{hmin}). The best predictor is in bold.

Predictor of f_q	Coefficients for 14 soils		Confidence interval from bootstrapping		Impact of a change of $\pm 0.08 \times 10^6 \text{ J m}^{-3} \text{ K}^{-1}$ in C_{hmin}	
	a_0	a_1	a_0	a_1	a_0	a_1
m_{sand} / m_{SOM}	0.12	0.0134	[0.10,0.14]	[0.012,0.014]	[0.11,0.13]	[0.013,0.013]
m_{sand}^*	0.08	0.944	[0.00,0.11]	[0.85,1.40]	[0.07,0.09]	[0.919,0.966]
m_{sand}	0.15	0.572	[0.08,0.17]	[0.54,0.94]	[0.14,0.17]	[0.55,0.56]
$1 - \theta_{sat} - f_{sand}$	0.73	-1.020	[0.71,0.89]	[-1.38, -0.99]	[0.70,0.73]	[-1.00, -0.99]

612 (*) only m_{sand} values smaller than 0.6 kg kg^{-1} are used in the regression

613

613 **Table 4** – Scores of four pedotransfer functions of f_q for 14 soils of this study, together with the
 614 scores obtained by bootstrapping, without the sandy SBR soil. The MAE score of these
 615 pedotransfer functions for three Chinese soils of Lu et al. (2007) for which $m_{\text{sand}}/m_{\text{SOM}} < 40$ is
 616 given. The best predictor and the best scores are in bold.

Predictor of f_q	Regression scores			Bootstrap scores			Scores without SBR (and MAE for 3 Lu soils)		
	r^2	RMSD ($\text{m}^3 \text{m}^{-3}$)	MAE ($\text{m}^3 \text{m}^{-3}$)	r^2	RMSD ($\text{m}^3 \text{m}^{-3}$)	MAE ($\text{m}^3 \text{m}^{-3}$)	r^2	RMSD ($\text{m}^3 \text{m}^{-3}$)	MAE ($\text{m}^3 \text{m}^{-3}$)
$m_{\text{sand}} / m_{\text{SOM}}$	0.77	0.067	0.053	0.72	0.074	0.059	0.62	0.070	0.057 (0.135)
m_{sand}^*	0.74	0.072	0.052	0.67	0.126	0.100	0.56	0.075	0.056 (0.071)
m_{sand}	0.67	0.081	0.060	0.56	0.121	0.084	0.56	0.075	0.056 (0.086)
$1 - \theta_{\text{sat}} - f_{\text{sand}}$	0.65	0.084	0.064	0.56	0.102	0.079	0.45	0.084	0.061 (0.158)

617 (*) only m_{sand} values smaller than 0.6 kg kg^{-1} are used in the regression

618
 619
 620
 621
 622
 623

623 **Table 5** – Ability of the Eqs. (10)-(13) empirical model to estimate λ_{sat} values for 14 soils and
624 impact of changes in gravel and SOM volumetric content: $f_{\text{gravel}} = 0 \text{ m}^3\text{m}^{-3}$ and $f_{\text{SOM}} = 0.013$
625 m^3m^{-3} (the smallest f_{SOM} value, observed for CBR). r^2 values smaller than 0.60, RMSD values
626 higher than $0.20 \text{ Wm}^{-1}\text{K}^{-1}$, and mean bias values higher (smaller) than $+0.10$ (-0.10) are in bold.

Model configuration	Predictor of f_q	r^2	RMSD ($\text{Wm}^{-1}\text{K}^{-1}$)	Mean bias ($\text{Wm}^{-1}\text{K}^{-1}$)
Model using θ_{sat} observations	$m_{\text{sand}} / m_{\text{SOM}}$	0.86	0.14	+0.01
	m_{sand}^*	0.83	0.15	-0.01
	m_{sand}	0.81	0.16	-0.03
	$1 - \theta_{\text{sat}} - f_{\text{sand}}$	0.82	0.16	-0.03
Full model using θ_{satMOD} (Eqs. (13))	$m_{\text{sand}} / m_{\text{SOM}}$	0.85	0.14	+0.03
	m_{sand}^*	0.85	0.14	-0.03
	m_{sand}	0.84	0.15	-0.03
	$1 - \theta_{\text{sat}} - f_{\text{sand}}$	0.82	0.16	-0.02
same with: $f_{\text{SOM}} = 0.013 \text{ m}^3\text{m}^{-3}$	$m_{\text{sand}} / m_{\text{SOM}}$	0.57	0.35	+0.20
	m_{sand}^*	0.83	0.15	+0.00
	m_{sand}	0.81	0.16	-0.02
	$1 - \theta_{\text{sat}} - f_{\text{sand}}$	0.83	0.15	-0.02
same with: $f_{\text{gravel}} = 0 \text{ m}^3\text{m}^{-3}$	$m_{\text{sand}} / m_{\text{SOM}}$	0.87	0.19	-0.12
	m_{sand}^*	0.70	0.23	+0.11
	m_{sand}	0.79	0.17	+0.04
	$1 - \theta_{\text{sat}} - f_{\text{sand}}$	0.81	0.17	+0.05
same with: $f_{\text{SOM}} = 0.013 \text{ m}^3\text{m}^{-3}$ and $f_{\text{gravel}} = 0 \text{ m}^3\text{m}^{-3}$	$m_{\text{sand}} / m_{\text{SOM}}$	0.63	0.31	+0.16
	m_{sand}^*	0.52	0.36	+0.24
	m_{sand}	0.59	0.29	+0.16
	$1 - \theta_{\text{sat}} - f_{\text{sand}}$	0.70	0.25	+0.16

(*) only m_{sand} values smaller than 0.6 kg kg^{-1} are used in the regression

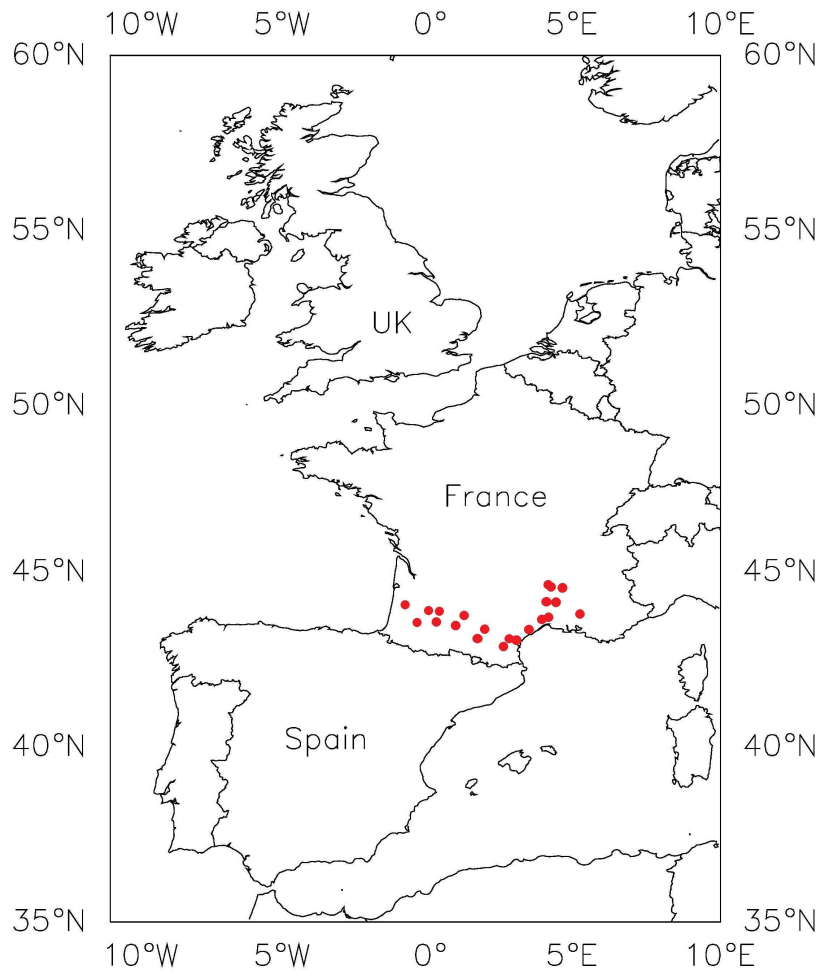
627
628
629
630

630 **Table 6** – Pedotransfer functions of f_q for 7 soils of Lu et al. (2007) with $m_{\text{sand}}/m_{\text{SOM}} > 40$. The
 631 best predictor and the best scores are in bold.

Predictor of f_q	Regression scores for 7 Lu soils with $m_{\text{sand}}/m_{\text{SOM}} > 40$			Coefficients	
	r^2 (<i>p-value</i>)	RMSD (m^3m^{-3})	MAE (m^3m^{-3})	a_0	a_1
$m_{\text{sand}} / m_{\text{SOM}}$	0.40 (0.13)	0.089	0.075	0.20	0.000148
m_{sand}^*	0.82 (0.005)	0.073	0.054	0.07	0.425
m_{sand}	0.82 (0.005)	0.048	0.042	0.04	0.386
$1 - \theta_{\text{sat}} - f_{\text{sand}}$	0.81 (0.006)	0.050	0.043	0.44	-0.814

(*) only m_{sand} values smaller than 0.6 kg kg^{-1} are used in the regression

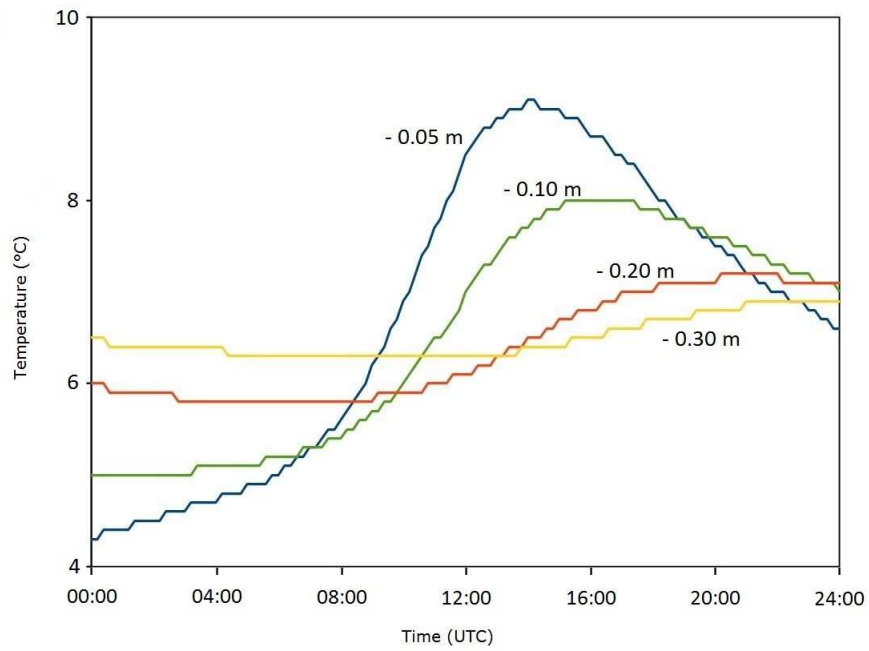
632
 633
 634
 635



636
637
638
639
640
641
642
643
644
645
646
647
648

Fig. 1 – Location of the 21 SMOSMANIA stations in southern France.

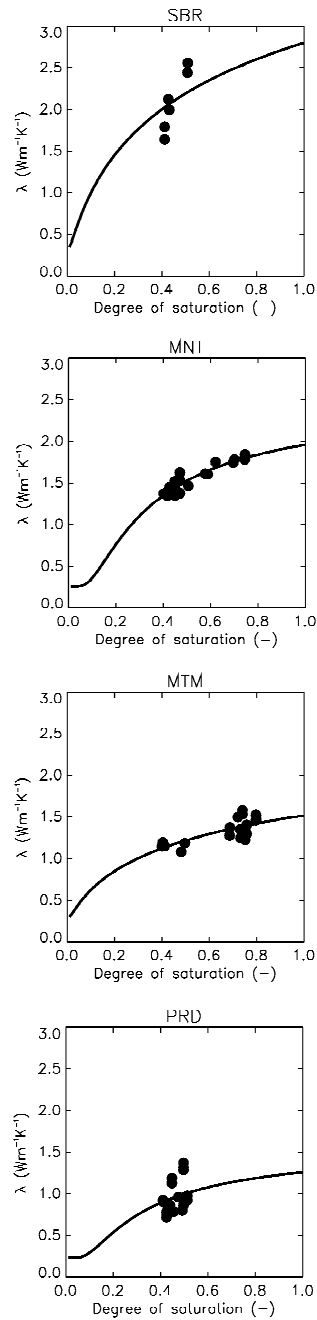
649
650
651
652
653



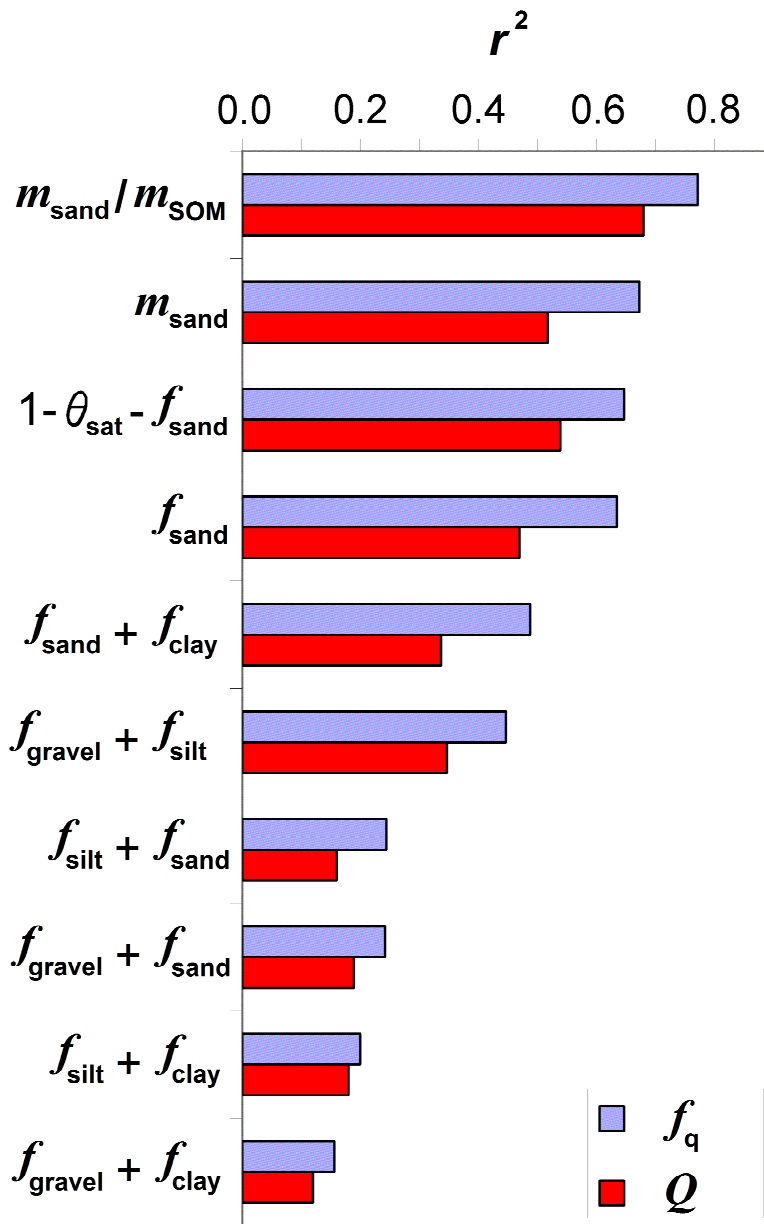
654
655
656
657
658
659
660
661
662
663

Fig. 2 – Soil temperature measured at the Saint-Félix-de-Lauragais (SFL) station on 23 February 2015, at depths of 0.05, 0.10, 0.20, and 0.30 m. Levelling is due to the low resolution of the temperature records (0.1°C).

664
665

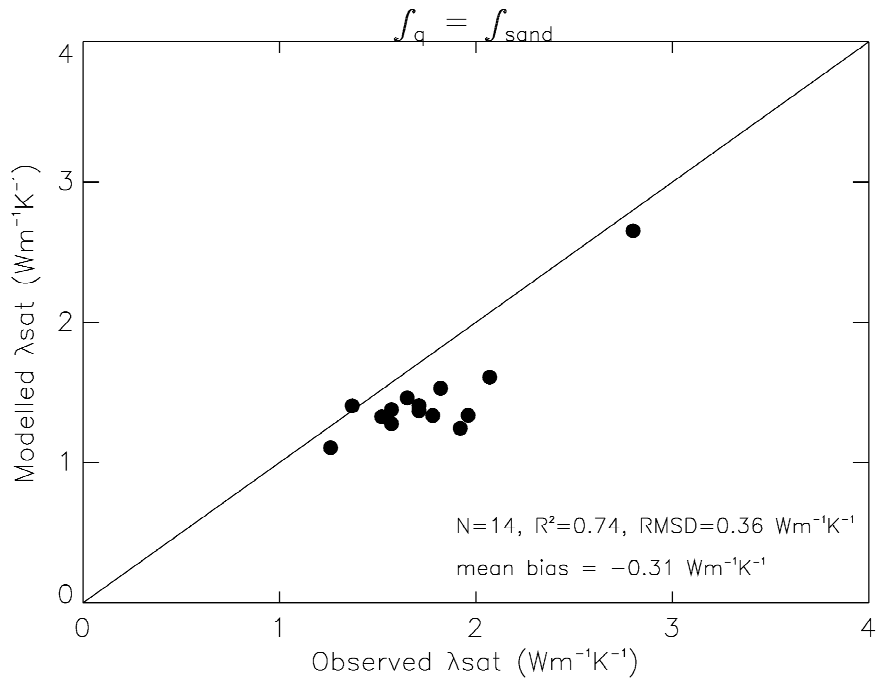


666
667 **Fig. 3** – Retrieved λ values (dark dots) vs. the observed degree of saturation of the soil, at a
668 depth of 0.10 m, for (from top to bottom) Sabres (SBR), Montaut (MNT), Mouthoumet (MTM),
669 and Prades-le-Lez (PRD), together with simulated λ values from dry to wet conditions (dark
670 lines).
671
672

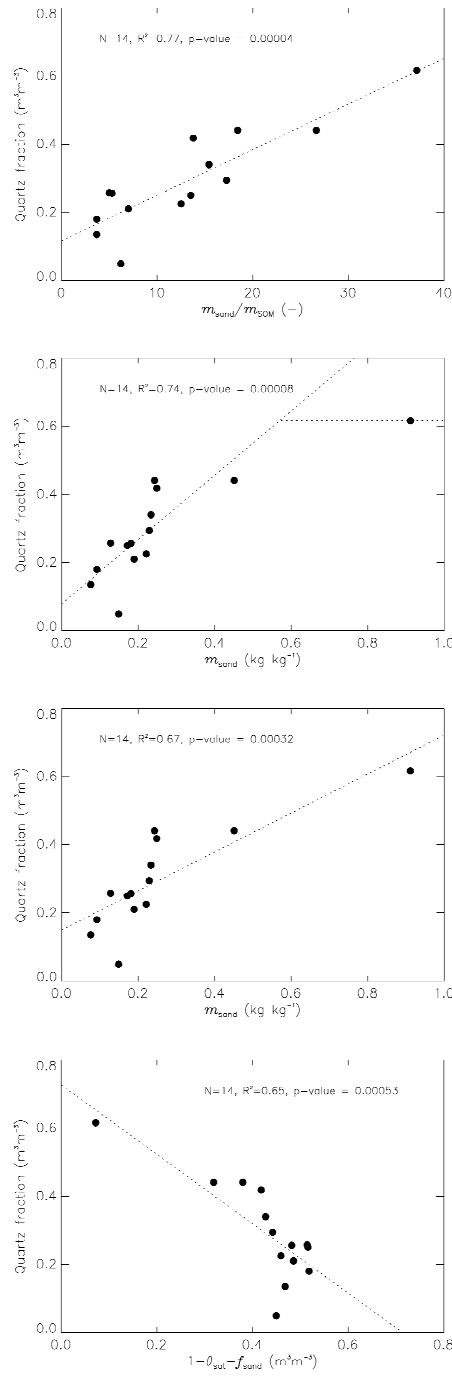


672
673
674
675

Fig. 4 – Fraction of variance (r^2) of gravimetric and volumetric fraction of quartz (Q and f_q , red and blue bars, respectively) explained by various predictors.

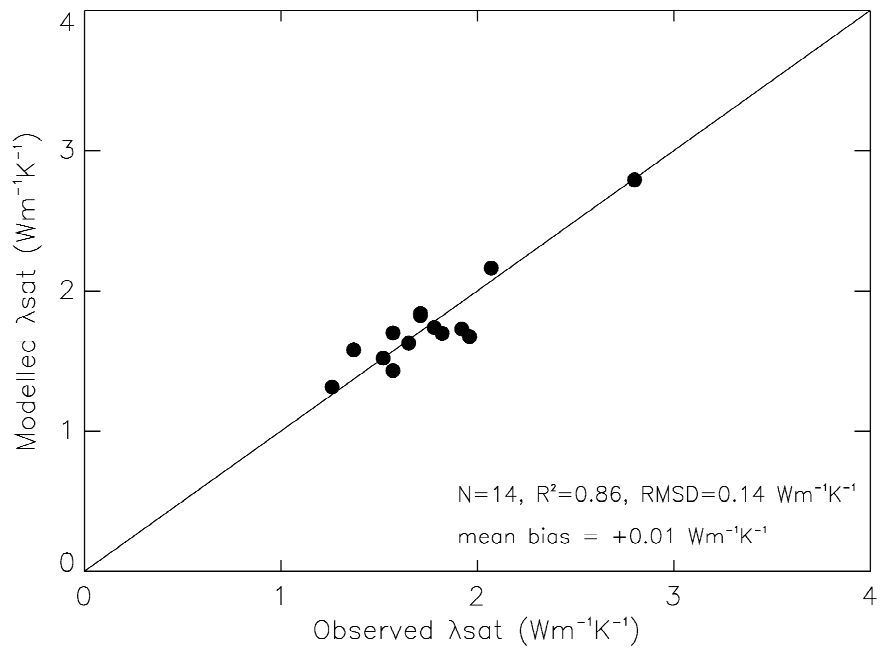


676
 677 **Fig. 5** – λ_{satMOD} values derived from volumetric quartz fractions f_q assumed equal to f_{sand} , using
 678 observed θ_{sat} values, vs. λ_{sat} retrievals.
 679

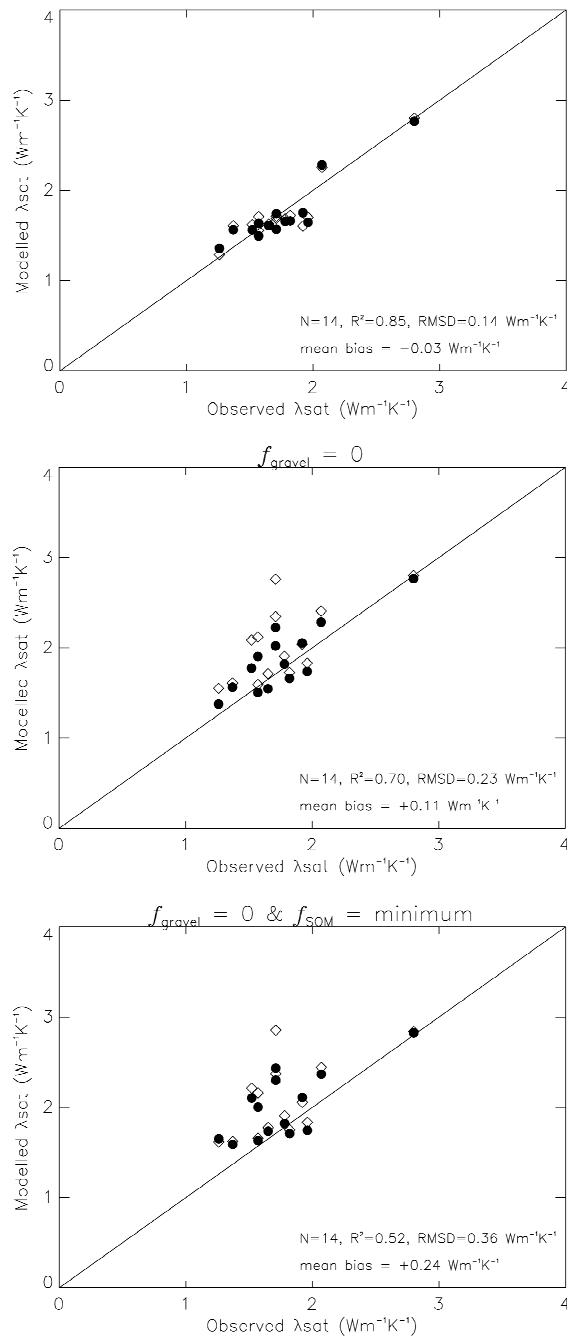


679
680
681
682
683

Fig. 6 – Pedotransfer functions for quartz: f_q retrievals (dark dots) vs. the four predictors of f_q given in Table 3. The modelled f_q values are represented by the dashed lines.

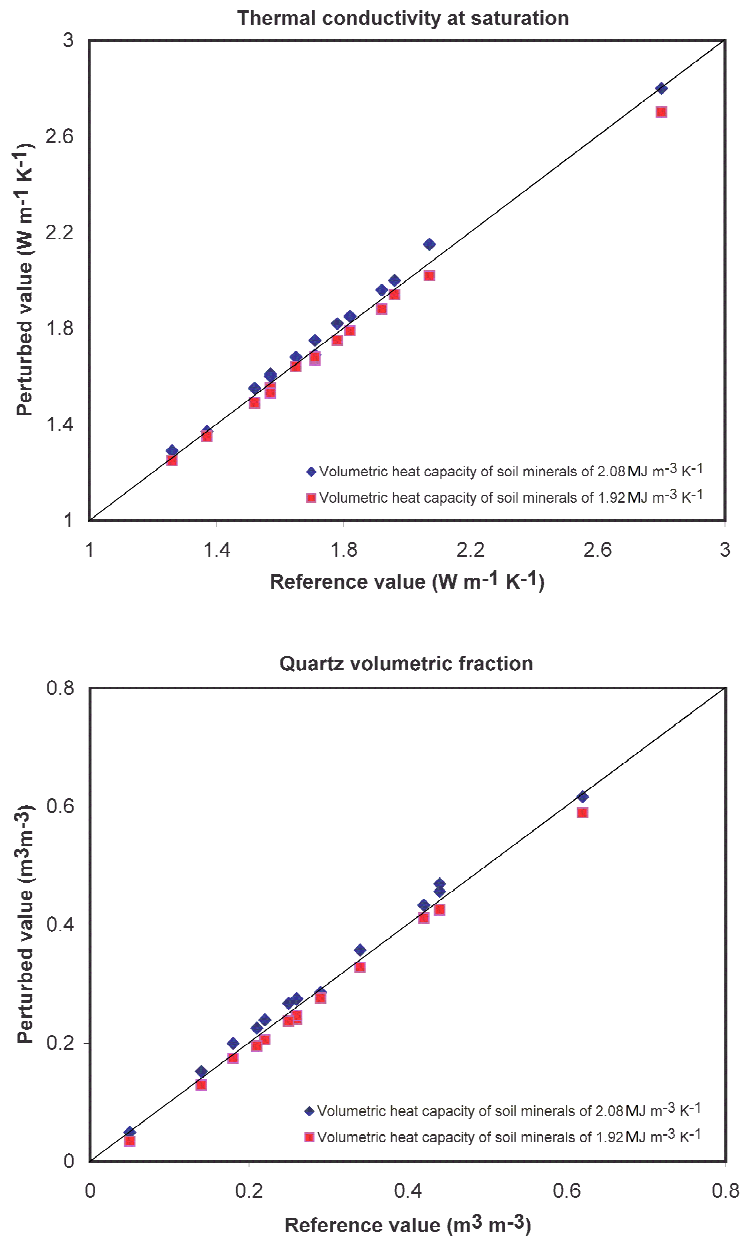


683
 684 **Fig. 7** – $\lambda_{\text{sat}MOD}$ values derived from the $m_{\text{sand}} / m_{\text{SOM}}$ pedotransfer function for the volumetric
 685 quartz fractions, using observed θ_{sat} values, vs. λ_{sat} retrievals.
 686



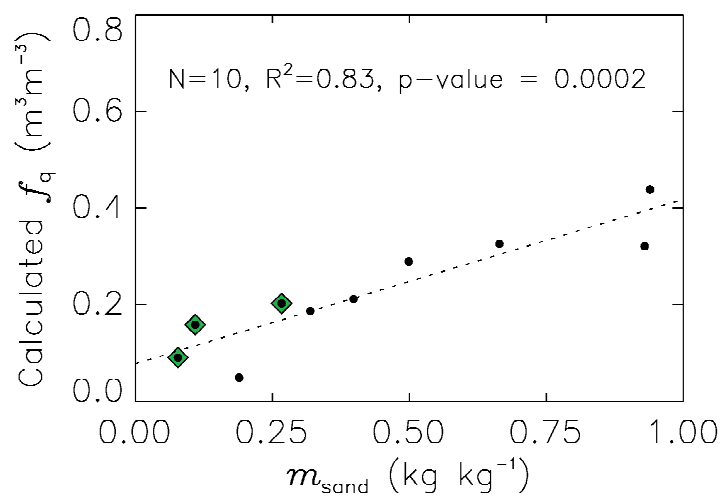
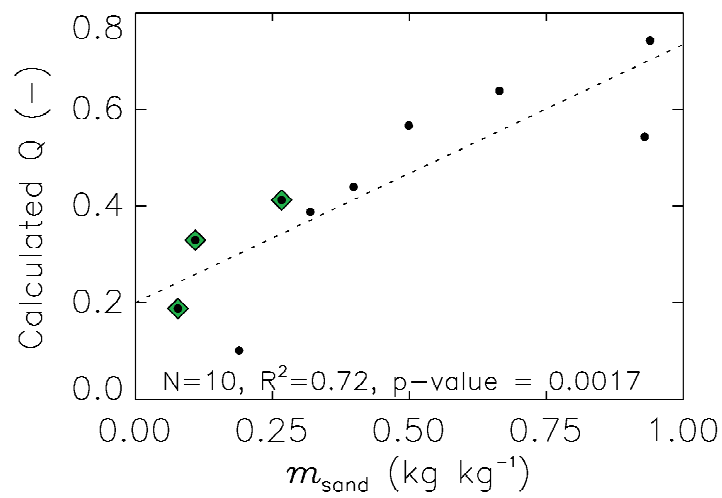
688
 689
 690
 691
 692
 693
 694
 695

Fig. 8 – λ_{satMOD} values derived from the m_{sand}^* pedotransfer function for the volumetric quartz fractions, using θ_{satMOD} (Eqs. (13)) or the observed θ_{sat} (dark dots and opened diamonds, respectively), vs. λ_{sat} retrievals: (top) full model, (middle) $f_{SOM} = 0.013 m^3 m^{-3}$, (bottom) $f_{SOM} = 0.013 m^3 m^{-3}$ and $f_{gravel} = 0 m^3 m^{-3}$. Scores are given for the θ_{satMOD} configuration.



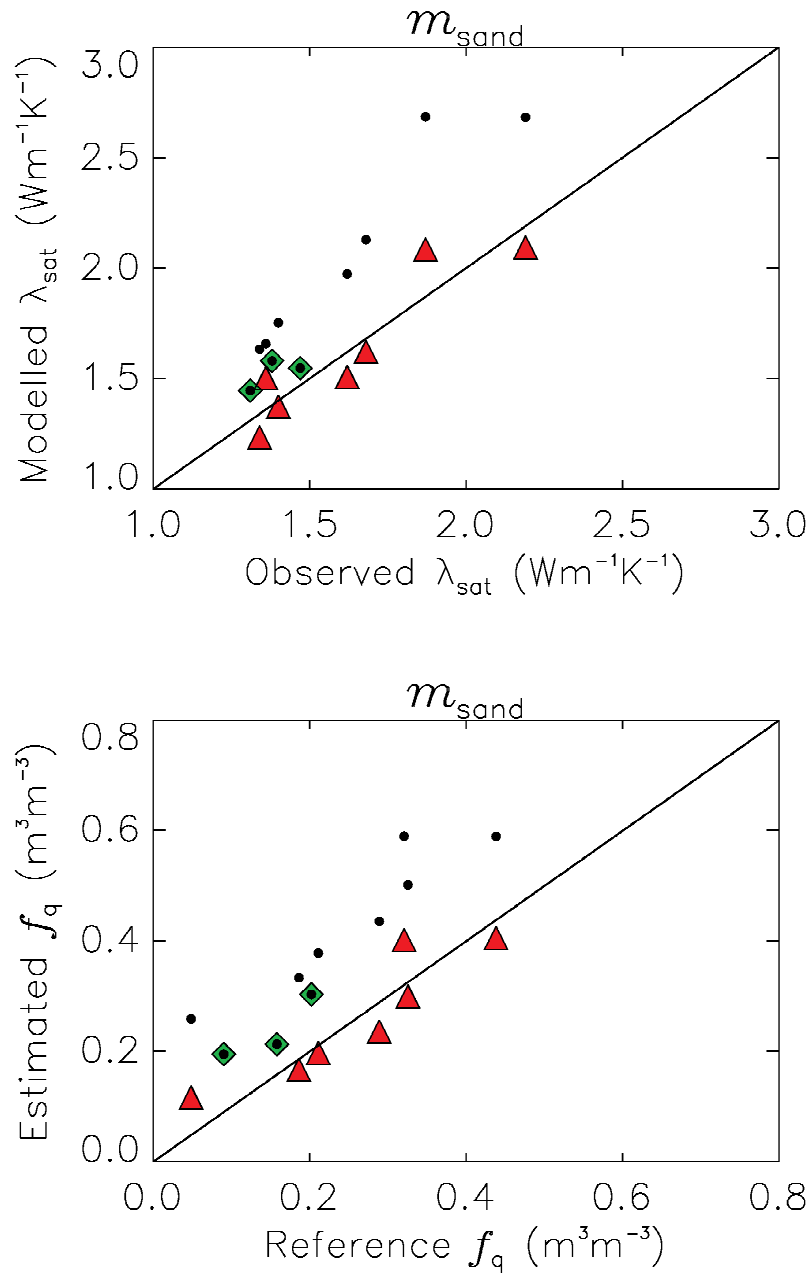
696
 697
 698
 699
 700

Fig. 9 – Impact of using values of $C_{hmin} = 1.92\ MJ\ m^{-3}\ K^{-1}$ and $C_{hmin} = 2.08\ MJ\ m^{-3}\ K^{-1}$ instead of $C_{hmin} = 2.0\ MJ\ m^{-3}\ K^{-1}$ on (top) the retrieved λ_{sat} , (bottom) the volumetric fraction of quartz.



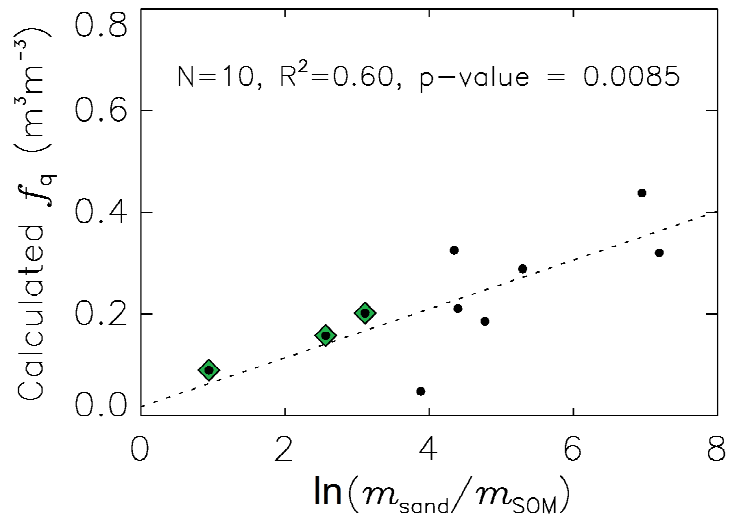
701
702
703
704
705
706
707
708
709

Fig. 10 – Gravimetric and volumetric fraction of quartz (top and bottom, respectively) derived from the λ_{sat} observations of Lu et al. (2007) for 10 soils given by Tarnawski et al. (2009), vs. the gravimetric fraction of sand m_{sand} . The three soils for which $m_{\text{sand}}/m_{\text{SOM}} < 40$ are indicated by green diamonds. The dashed lines represent the regression equations based on all soils: $Q = 0.20 + 0.54 m_{\text{sand}}$ and $f_q = 0.08 + 0.34 m_{\text{sand}}$.



709
710

711 **Fig. 11** – Estimated λ_{sat} and volumetric fraction of quartz f_q (top and bottom, respectively) vs.
712 values derived from the λ_{sat} observations of Lu et al. (2007) given by Tarnawski et al. (2009) for
713 10 Chinese soils, using the gravimetric fraction of sand m_{sand} as a predictor of f_q . Dark dots
714 correspond to the estimations obtained using the m_{sand} pedotransfer function for southern France
715 and the three soils for which $m_{\text{sand}}/m_{\text{SOM}} < 40$ are indicated by green diamonds. Red triangles
716 correspond to the estimations obtained using the m_{sand} pedotransfer function for the seven soils
717 for which $m_{\text{sand}}/m_{\text{SOM}} > 40$.
718



719
720

721 **Fig. 12** – Volumetric fraction of quartz derived from the λ_{sat} observations of Lu et al. (2007)
722 given by Tarnawski et al. (2009), vs. the logarithm of the $m_{\text{sand}} / m_{\text{SOM}}$ ratio. The three soils for
723 which $m_{\text{sand}}/m_{\text{SOM}} < 40$ are indicated by green diamonds. The dashed line represents the
724 regression equation: $f_q = 0.02 + 0.048 \ln(m_{\text{sand}}/m_{\text{SOM}})$.

725
726